Admittance spectroscopy of GeSi-based quantum dot systems: Experiment and theory

Xi Li,[1] W. Xu,[2,3,*] Shihai Cao,[1] Qijia Cai,[1] and Fang Lu[1,†]

[1]*Department of Physics, Surface Physics Laboratory, Fudan University, Shanghai 200433, People's Republic of China*
[2]*Department of Theoretical Physics, Research School of Physical Sciences & Engineering, Australian National University, Canberra, Australian Capital Territory 0200, Australia*
[3]*Institute of Solid State Physics, Chinese Academy of Sciences, Hefei 230031, People's Republic of China*

A combined experimental and theoretical study is carried out in examining the important features of the admittance spectroscopy (AS) of self-assembled GeSi quantum dot (QD) systems. In the experimental component of the study, we measure the dependence of the AS on size of the GeSi QDs. From such measurements, we determine the emission rate and activation energy of the carriers in different QDs. Theoretically, we develop a simple approach to understand and reproduce those observed experimentally. It is found both experimentally and theoretically that with increasing size of the QDs, the peak of the AS shifts to higher-temperature regime, the activation energy of the carriers increases and the emission rate of the system decreases. These interesting phenomena can be well explained by the fact that in GeSi-based QD systems, the AS is mainly induced by zero-dimensional to three-dimensional transition through hole interactions with acoustic phonons via deformation potential coupling.

I. INTRODUCTION

The state-of-the-art material engineering and nanofabrication techniques have made it possible to realize advanced semiconductor devices at atomic scales, such as quantum dots (QDs) in which the electron or hole motion is quantized in all spatial directions and the conducting carriers are confined within the nanometer distances. Such systems can behave as artificial atoms and, therefore, be applied as advanced electronic and optical devices, such as memory chip,[1] quantum computer,[2] quantum cryptography,[3] quantum-dot laser,[4] to mention but a few. At present, both electrical and optical techniques have been widely used in the characterization and investigation of GaAs-, InGaAs-, and GeSi-based QD systems.[5] In particular, in recent years the admittance spectroscopy (AS) has become a powerful tool in the electrical characterization of InGaAs- (Refs. 6–8) and GeSi-based[9,10] QD structures. When a QD is subjected to an ac electric field, the conducting carriers in the dot can be emitted to the continuum states of the systems and the carriers in the continuum states can also be captured into the bound states in the dot with the assistance of electronic scattering mechanisms. In such a case, the number of carriers in the dot alters with the intensity and frequency of the applied ac field and, as a result, the conductance and capacitance can be measured from the system. Hence, the AS measurement can be applied to determine important device parameters such as the activation energy of the carriers, the strength of the quantum confinement, the energy level structure, the emission and capture rates, etc. The experimental results obtained very recently[6–10] have indicated that in InGaAs- and GeSi-based QD systems in which the conducting carriers are, respectively, electrons and holes, the electronic emission rate is about $1/ms$−$1/\mu s$ so that the AS can be measured under the action of the ac fields with frequencies around $1\ kHz$−$1\ MHz$ at a temperature range from 50 K to room temperature. Consequently, the AS is a simple, conventional

and powerful technique which measures electrically the electronic and transport properties of InGaAs- and GeSi-based quantum dot systems.

In this work, we intend examining experimentally the effect of the size of self-assembled GeSi QDs on features of the AS. It is known that the AS in a QD system is mainly induced by charge transfer in different states, especially between bound and continuum states, due to the presence of the electrical driving fields and electronic scattering mechanisms. The variation of the size of the dot changes the strength of the quantum confinement to the carriers in the dot and, therefore, alters the possibility for electronic transition in different energy levels. Hence, it is expected that the features of the AS in QD systems are sensitive to the size of the QD. In this study, the GeSi QDs are grown by the standard technique of self-assemble on the basis of molecular-beam epitaxy (MBE) growth. The AS measurements are undertaken by a conventional transport experiment in the presence of the ac driving fields.

In sharp contrast to quite intensive experimental work in using AS for studying different QD systems,[6–10] very little theoretical work regarding the AS in QDs has been reported so far. At present, there is a lack of corresponding theory in analyzing and understanding the related experimental findings. To fill this gap, in this study, we develop a tractable and systematic theoretical approach to calculate the conductance and capacitance in conjunction with the AS measurement for GeSi-based QD systems. Very recently, we have proposed a simple theory to study the AS in GeSi-based quantum well systems.[12] This theoretical approach is based on a mass-balance equation derived from the semiclassic Boltzmann equation and the obtained theoretical results agree very well with those measured experimentally.[12] In the present study, we generalize this approach developed for a GeSi quantum well to the case of self-assembled GeSi QDs. The validity of this model calculation is examined by those obtained from our current experimental measurements. On the other hand, we can also use those obtained theoretically to understand

TABLE I. Sample growth parameters (left panel) and the AS peak position and peak half-width obtained experimentally and theoretically (right panel).

Sample No.	Ge content in QD x	Growth temperature (°C)	Ge layer width (Å)	QD diameter (Å)	QD height (Å)	QD areal density (10^8 cm^{-2})	Peak position (expt. vs theor.) (K)	Peak half-width (expt. vs theor.) (K)
A	0.75	500	13	130	30	8	166 vs 165	28 vs 20
B	0.75	510	15	200	35	3	184 vs 182	30 vs 22
C	0.75	500	17	600	45	1	233 vs 232	31 vs 26

our experimental findings and to reproduce those observed experimentally. Thus, this combined experimental and theoretical study can achieve an in-depth understanding of the features of the AS in GeSi-based QDs.

In this paper, the details of the sample growth, device fabrication, experimental setup, and measurement are described in Sec. II. In Sec. III, we present the theoretical approach to calculate the conductance and capacitance in conjunction with AS measurement in self-assembled GeSi QDs. The experimental and theoretical results obtained from this study are presented and discussed in Sec. IV. The main conclusions drawn from the present study are summarized in Sec. V.

II. SAMPLES AND MEASUREMENTS

The samples used in the present study are prepared by the techniques of self-assemble on the basis of the MBE growth. The growth of the GeSi islands is achieved in an ultrahigh-vacuum MBE system (Riber Eva-32) with two electron-beam evaporators as Ge and Si sources. The base pressure of the growth system is less than 5×10^{-10} Torr. A *p*-type Si (001) wafer is employed as substrate with a resistivity of about $1-10$ Ω cm. The substrate is chemically cleaned using the Shiraki method.[13] The protecting oxide layer on the substrate is desorbed at 1000 °C for 10 min in the growth chamber. The temperature is then lowered to 500 °C and a 100-nm-thick Si buffer layer is grown with a growth rate of 0.1 nm/s to achieve an epitaxial surface. Afterward, three layers of Ge are deposited and these Ge layers are separated by 45-nm-thick Si spacer layers. The self-assembled GeSi dots are formed using the Stranski-Krastanov growth mode during which the Si diffuses into the QD layers. During the growth of the Si spacer layers, the Boron δ doping takes place with the concentration about 1×10^{16}/cm^{-3}. These δ-doped layers can provide conducting holes in the QDs. Here, a two-step growth method has been adopted in island growth at a rate of 0.02 nm/s and a temperature at about 500 °C in order to improve the uniformity of the GeSi islands. Finally, after depositing a Si cap layer with 320 nm thickness, the substrate temperature is immediately cooled down to room temperature and the GeSi QD sample is prepared.

In general, the size of self-assembled GeSi QDs relies on the growth temperature and the widths of the Ge layer and the Si spacer layer. Usually, the size of the GeSi QDs increases with the growth temperature and with the thickness

of the Ge layer.[14,15] In the present study, to investigate the effect of the size of the QDs on the AS, three samples (A, B, and C, as shown in Table I) are prepared at almost the same growth temperature and rate, the same Boron δ-doping layer, and the same Si spacer layers but with different widths of the Ge layers. Thus, the QD size is mainly determined by the thickness of the Ge layers. The quality and the size of the dots can be examined and determined by the transmission electron microscopy (TEM) and atomic force microscopy (AFM) with good accuracy. The cross-section TEM and the AFM images show a uniform spatial distribution of the dots, where the nonuniformity of the QD size is estimated to be less than 10%. The TEM and AFM images also show that these QDs have a roughly circular symmetry along the direction perpendicular to the growth direction. The sample growth parameters and the sample parameters are shown in Table I. For three samples A, B, and C with the Ge layer widths being, respectively, 13, 15, and 17 Å, the areal density of the QDs, the height of the QDs along the growth direction, and the QD diameter perpendicular to the growth direction shown in Table I are determined by the techniques of TEM and AFM. It can be found that the areal density of the QDs decreases with increasing size of the Dots. We note that the QD sizes and the areal densities of our samples are quite similar to those grown by other groups.[16] The Ge content in a GeSi dot shown in Table I is estimated by the Raman spectra, where the intensities of the Raman scattering induced by Si-Si, Si-Ge, and Ge-Ge optic-phonon modes are sensitive to the Ge composition.[17–19] From Table I, we see that with increasing slightly the thickness of the Ge layer, the size of the QD increases significantly along both the growth direction and the direction perpendicular to the growth direction, in line with those observed by other groups.[16]

To measure the AS, the QD devices are fabricated with a Schottky diode structure, where an Al electrode with the diameter of 1 mm without alloying is placed at the front side and an Ohmic contact is at the back side. In the present study, the admittance is measured along the growth direction, namely, the dc and ac fields are applied along the growth direction and the conductance and capacitance are measured along this direction as well. The conductance is measured by a commercial HP 4284A *LCR* meter which can also apply the dc and ac bias voltages to the sample systems. The measurements are carried out within a temperature range from 80 to 250 K in the presence of the weak ac voltage with a frequency $f = \omega/2\pi$ range from 1 kHz to 1 MHz provided by the 4284A *LCR* meter. The temperature of the measurement is applied by a thermocouple with a Keithley 2400 sourcem-
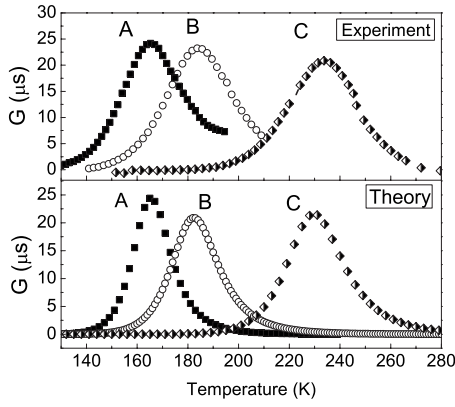
FIG. 1. Experimental (upper panel) and theoretical (lower panel) results for conductance as a function of temperature in GeSi-based QDs with different dot sizes (the lateral diameters in the xy plane are 13, 20, and 60 nm for, respectively, samples A, B, and C shown in Table I). The results are obtained by applying an ac field with a frequency $f=1$ MHz.

eter as the voltage indicator. Both meters are controlled by the computer through the IEEE-488 interfaces.

The results of the AS obtained for three samples with different QD diameters and heights are shown in Fig. 1 at a fixed ac field frequency. With the experimental data measured at different ac field frequencies, the emission rate λ_E and activation energy E_a of the carriers in the QD can be determined, respectively, by using

$$G = \frac{\kappa \lambda_E \omega^2}{\lambda_E^2 + \omega^2}, \tag{1}$$

and

$$\lambda_E = \beta T \exp(-E_a/k_B T), \tag{2}$$

where G is the measured conductance and κ and β are coefficients independent on temperature and ac field frequency. These equations will be obtained theoretically in the next section of the paper. With Eq. (1), the emission rate can be determined simply by one of the following experiments. (1) $\lambda_E \sim \omega_p$ with ω_p being the ac field frequency at which the peak of the conductance is observed at a fixed temperature in the measurement or (2) $\lambda_E \sim \omega$ at a temperature corresponding to the peak of the conductance when f is fixed in the measurement. The results of λ_E and E_a for different samples are shown, respectively, in Figs. 2 and 3.

From the above mentioned experimental setup and sample and measurement configurations, we know that the AS measured experimentally is mainly induced by electronic transition from zero-dimensional (0D) (or bound) states in the QD to the three-dimensional (3D) (or continuum) states of the sample system. In particular, because the applied ac and dc voltages in the measurements are along the growth direction, the electronic transition takes place along this direction as well.
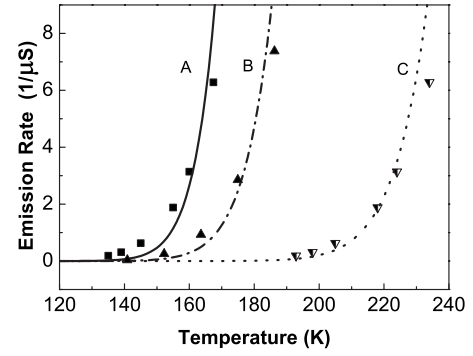
FIG. 2. Experimental (symbols) and theoretical (curves) results of the emission rate for different samples A, B, and C. The experimental results are obtained by applying the ac fields with different frequencies.

In the present study, we also carry out the capacitance-voltage (C-V) measurements for different QD samples. From these results, we can determine the effective carrier concentration in a QD along the direction of the lateral confinement through the relation[9,11]

$$N_c = \frac{C^3}{e \epsilon \epsilon_0 A^2 (-dC/dV)}, \tag{3}$$

where $C = \epsilon \epsilon_0 A / L_d$ is the capacitance with ϵ and ϵ_0 being, respectively, the material and vacuum dielectric constants, A is the area of the electrode, and L_d is the depletion length. This carrier density can be used to determine the filling factor ν of a QD, which is defined as the ratio of the carrier concentration N_c and the areal density of the dots N_d in the direction perpendicular to the growth direction. Using N_d obtained from TEM and AFM images and shown in Table I and N_c obtained from the C-V measurements, the filling factors are about 5–20 for samples A, B, and C shown in Table I. The filling factor ν connects directly to the characteristic frequency of a QD.[20]
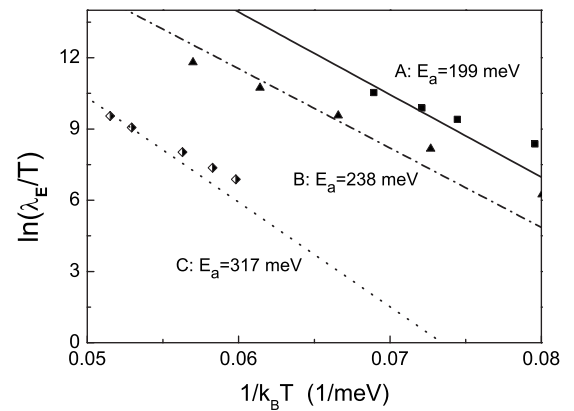
FIG. 3. Experimental (symbols) and theoretical (curves) results for $\ln(\lambda_E/T)$ as a function of $1/K_B T$ for different samples A, B, and C. Here, E_a is the activation energy and λ_E is the emission rate.

III. THEORETICAL APPROACH

In conjunction with the AS measurement of a GeSi-based QD system, our theoretical investigation can be undertaken on the basis of following considerations. (i) A dc gate voltage and an ac electric field are applied along the growth direction of the QD to measure the capacitance and conductance. The dc bias plays mainly a role in varying the hole subband structure in the QD, and the ac field can be taken as a driving field which alters the number of holes in the QD in the presence of the dc bias. (ii) The AS is a consequence of the carriers going in or out of QD driven by the small ac electric field applied to the QD. (iii) The change of the hole numbers in the QD is mainly due to transitions of holes from bound states (0D) to continuum states (emission process) or from continuum states (3D) to bound states in the dot (capture process). (iv) The transition of holes among different states is a consequence of the presence of the ac field and of the electronic scattering mechanisms.

A. Conductance and capacitance

In this section, we develop a general theory to study the conductance and capacitance in a QD system in conjunction with the AS measurement. For simplicity, we employ the semiclassic Boltzmann equation as the governing transport equation to calculate the AS induced by charge transfer between the bound and continuum states in a QD. Because the applied ac field in the admittance measurement is time dependent and we consider relatively high-temperature and low-density samples, we can start our calculation from time-dependent Boltzmann equation in nondegenerate statistics. For a hole in the continuum (3D) and bound (0D) states, the Boltzmann equations can be written, respectively, as

$$\frac{\partial f(\alpha_3, t)}{\partial t} = g_s \sum_{\alpha_0} [f(\alpha_0, t) W(\alpha_0; \alpha_3) - f(\alpha_3, t) W(\alpha_3; \alpha_0)]$$
$$+ g_s \sum_{\alpha_3'} [f(\alpha_3', t) W(\alpha_3'; \alpha_3) - f(\alpha_3, t) W(\alpha_3; \alpha_3')]$$
(4)

and

$$\frac{\partial f(\alpha_0, t)}{\partial t} = g_s \sum_{\alpha_3} [f(\alpha_3, t) W(\alpha_3; \alpha_0) - f(\alpha_0, t) W(\alpha_0; \alpha_3)]$$
$$+ g_s \sum_{\alpha_0'} [f(\alpha_0', t) W(\alpha_0'; \alpha_0) - f(\alpha_0, t) W(\alpha_0; \alpha_0')].$$
(5)

Here, α_0 and α_3 are quantum numbers to describe, respectively, the bound (or 0D) and continuum (or 3D) hole states, $f(\alpha_0, t)$ and $f(\alpha_3, t)$ are time-dependent distribution functions, respectively, for a hole at a 0D state α_0 and for a hole at a 3D state α_3, $g_s = 2$ counts for spin degeneracy, and $W(\alpha; \alpha')$ is the steady-state electronic transition rate for scattering of a hole from a state α to a state α'. The first term on the right-hand side of Eqs. (4) and (5) comes from electronic transition between the bound and continuum states, and the

second term is induced by scattering events within the bound or continuum states. Furthermore, the effect of hole interactions with scattering centers has been considered within the electronic transition rate, the effect of the dc bias has been included within the hole wave function and energy spectrum, and the effects of the ac field are implied in the time-dependent hole distribution functions. Thus, to avoid double counting, the force terms caused by the ac and dc fields do not show on the left-hand side of the Boltzmann equation. In general, there is no simple and analytical solution to Eqs. (4) and (5). In this work, we apply the usual balance-equation approach to solve the problem.[21] The advantage of this approach is that one can detour the difficulties of solving Boltzmann equation directly and the interested physical properties can be calculated approximately on the basis of the statistical distribution functions.[21] For the first moment, the mass-balance equation (or rate equation) can be derived by multiplying $g_s \Sigma_{\alpha_3}$ and $g_s \Sigma_{\alpha_0}$ to both sides of, respectively, Eqs. (4) and (5). Thus, we can obtain a rate equation

$$dQ_0(t)/dt = Q_3(t)\lambda_C - Q_0(t)\lambda_E,$$
(6)

and the condition of hole number conservation:

$$dQ_0(t)/dt = -dQ_3(t)/dt.$$

Here, $Q_0(t) = g_s \Sigma_{\alpha_0} f(\alpha_0, t)$ is the hole number in the bound states in the QD, $Q_3(t) = g_s V \Sigma_{\alpha_3} f(\alpha_3, t)$ is the hole number in the continuum states in the system with V being the volume of a QD,

$$\lambda_C = \frac{4}{Q_3(t)} \sum_{\alpha_0, \alpha_3} f(\alpha_3, t) W(\alpha_3; \alpha_0)$$
(7)

is the capture rate which measures the strength for transition of holes from the 3D states to the 0D states, and

$$\lambda_E = \frac{4}{Q_0(t)} \sum_{\alpha_0, \alpha_3} f(\alpha_0, t) W(\alpha_0; \alpha_3)$$
(8)

is the emission rate which measures the strength for transition of holes from bound states (0D) to continuum states (3D). Equation (6) reflects a fact that the change of the charge number in the bound states of a QD is induced by electronic scattering between 0D and 3D states. The condition of hole number conservation implies that the increase in the hole numbers in the continuum states comes from the decrease in the hole numbers in the bound states of a QD. Under the action of the ac field, a charge transfer can be achieved in the QD system. For example, if holes in the 0D states are emitted into the 3D states within the first half circle of the ac field, holes in the 3D states are captured into the 0D states within the second half circle of the ac field. Thus, a current circuit can be formed due to this kind of change transfer. Using Eq. (6), the current in the circuit is

$$I(t) = -dQ_0(t)/dt = Q_0(t)\lambda_E - Q_3(t)\lambda_C.$$
(9)

Under the action of an ac driving field $\delta V_t = V_0 e^{i\omega t}$, with V_0 and ω being, respectively, the strength and frequency of the ac field, the hole number at the 0D states in a QD is the difference between the mobile hole number $\delta Q_0(t)$ and the

emitted hole number in a field circle $\Delta Q_0(t) = \int_0^t dt I(t)$, namely, $Q_0(t) = \delta Q_0(t) - \Delta Q_0(t)$. For the case of a weak ac field so that a linear response is achieved, we have $\delta Q_0(t) = \kappa \delta V_t = \kappa V_0 e^{i\omega t}$ and $I(t) = I_0 e^{i\omega t}$. Here, a coefficient

$$\kappa = \frac{\delta Q_0(t)}{\delta V_t} = \frac{dQ_0(t)}{dV_t} = g_s e \sum_{\alpha_0} \frac{\partial f(E_{\alpha_0})}{\partial \mu_t} \frac{\partial \mu_t}{\partial V_t}$$

can be evaluated by assuming that the effect of the ac field is mainly on the Fermi energy (or chemical potential) μ_t of the system, where $f(x)$ is the Fermi-Dirac function and E_{α_0} is the energy spectrum for a hole in a bound state. We note that for a weak ac field which results in a linear response $\partial \mu_t / \partial V_t = e$, we have

$$\kappa = \frac{2e^2}{k_B T} \sum_{\alpha_0} f(E_{\alpha_0})[1 - f(E_{\alpha_0})]. \tag{10}$$

Inserting these results into Eq. (9), we get

$$I(t) = \left[\kappa V_0 e^{i\omega t} - \int_0^t dt I(t) \right] \lambda_E - Q_3(t)\lambda_C$$

and, as a result,

$$\dot{I}(t) = [i\omega \kappa V_0 e^{i\omega t} - I(t)]\lambda_E - \dot{Q}_3(t)\lambda_C. \tag{11}$$

When the system is in equilibrium, the total hole number in the system should be conserved so that

$$\dot{Q}_0(t) = -\dot{Q}_3(t) = -I(t).$$

Thus, Eq. (11) can be solved analytically. After using the definition for conductance $\mathcal{G} = I_0/V_0$ and for capacitance $\mathcal{C} = -dQ_0(t)/dV_t = -[dQ_0(t)/dt]/[dV_t/dt]$, we obtain

$$\mathcal{G} = \frac{i\kappa\omega\lambda_E}{\lambda_E + \lambda_C + i\omega} \quad \text{and} \quad G = \text{Re } \mathcal{G} = \frac{\kappa\omega^2\lambda_E}{(\lambda_E + \lambda_c)^2 + \omega^2}, \tag{12}$$

and

$$\mathcal{C} = \frac{\kappa\lambda_E}{\lambda_E + \lambda_C + i\omega} \quad \text{and} \quad C = \text{Re } \mathcal{C} = \frac{\kappa\lambda_E(\lambda_E + \lambda_C)}{(\lambda_E + \lambda_c)^2 + \omega^2}. \tag{13}$$

For case where the measurement is carried out at a relatively high-temperature for a relatively low carrier density sample, we can employ a statistical energy distribution such as the Maxwillian as the distribution function for a hole in the QD. Taking $f(\alpha, t) = C(t)e^{-E_\alpha/k_B T}$ where $c(t)$ is a normalization factor determined by $Q_0(t) = C_0(t)g_s\sum_{\alpha_0} e^{-E_{\alpha_0}/k_B T}$ for a 0D hole and $Q_3(t) = C_3(t)Vg_s\sum_{\alpha_3} e^{-E_{\alpha_3}/k_B T}$ for a 3D hole, the capture and emission rates become, respectively,

$$\lambda_C = \frac{4}{A_3 V} \sum_{\alpha_0, \alpha_3} e^{-E_{\alpha_3}/k_B T} W(\alpha_3; \alpha_0) \tag{14}$$

and

$$\lambda_E = \frac{4}{A_0} \sum_{\alpha_0, \alpha_3} e^{-E_{\alpha_0}/k_B T} W(\alpha_0; \alpha_3), \tag{15}$$

which are time independent, with E_{α_i} being the energy spectrum for a hole at a state i and $A_i = g_s\sum_{\alpha_i} e^{-E_{\alpha_i}/k_B T}$. If the electronic transition rate $W(\alpha; \alpha')$ is known, we can calculate the emission and capture rates induced by the corresponding transition events and then calculate the conductance and capacitance.

B. GeSi-based quantum dot systems

It is known that in a GeSi-based QD, light and heavy holes are conducting carriers. At relatively high temperatures, the hole-phonon scattering is the principle mechanism for relaxation of excited holes in GeSi-based material systems. In this study, we consider a hole-phonon system with a Hamiltonian

$$H = H_h + H_p + H_{h-p}, \tag{16}$$

where $H_h = \mathbf{P}^2/2m^* + U(x, y, z)$ is the single-particle Hamiltonian for a hole, where $\mathbf{P} = (p_x, p_y, p_z)$ with $p_x = -i\hbar\partial/\partial x$ being the momentum operator along the x direction, m^* is the effective mass for a hole in the system, and $U(x, y, z)$ is the confinement potential for a hole in the dot, $H_p = \sum_{\mathbf{Q}} \hbar\omega_Q b_{\mathbf{Q}}^\dagger b_{\mathbf{Q}}$ is the phonon Hamiltonian, where $\mathbf{Q} = (q_x, q_y, q_z)$ is the phonon wave vector and $b_{\mathbf{Q}}^\dagger$ ($b_{\mathbf{Q}}$) is the creation (annihilation) operator for a phonon, and $H_{h-p} = \sum_{\mathbf{Q}} (V_{\mathbf{Q}} e^{i\mathbf{Q}\cdot\mathbf{R}} b_{\mathbf{Q}} + V_{\mathbf{Q}}^* e^{-i\mathbf{Q}\cdot\mathbf{R}} b_{\mathbf{Q}}^\dagger)$ is the hole-phonon interaction Hamiltonian, where $\mathbf{R} = (x, y, z)$ and $V_{\mathbf{Q}}$ is the strength of the hole-phonon coupling. Taking the hole-phonon interaction Hamiltonian as a perturbation, the electronic transition rate induced by hole-phonon coupling in a QD can be derived using Fermi golden rule, which reads

$$W(\alpha_0; \alpha_3) = \frac{2\pi}{\hbar} \sum_{\mathbf{Q}} \begin{bmatrix} N_Q \\ N_Q + 1 \end{bmatrix} |\langle \alpha_3 | e^{i\mathbf{R}\cdot\mathbf{Q}} | \alpha_0 \rangle|^2 |V_{\mathbf{Q}}|^2$$
$$\times \delta(E_{\alpha_0} - E_{\alpha_3} \pm \hbar\omega_Q) \tag{17}$$

for transition from a bound state $|\alpha_0\rangle$ to a continuum state $|\alpha_3\rangle$, and

$$W(\alpha_3; \alpha_0) = \frac{2\pi}{\hbar} \sum_{\mathbf{Q}} \begin{bmatrix} N_Q \\ N_Q + 1 \end{bmatrix} |\langle \alpha_0 | e^{i\mathbf{R}\cdot\mathbf{Q}} | \alpha_3 \rangle|^2 |V_{\mathbf{Q}}|^2$$
$$\times \delta(E_{\alpha_3} - E_{\alpha_0} \pm \hbar\omega_Q) \tag{18}$$

for transition from a continuum state $|\alpha_3\rangle$ to a bound state $|\alpha_0\rangle$. Here, the upper (lower) case refers to absorption (emission) of a phonon, $N_Q = [1 - e^{\hbar\omega_Q/k_B T}]^{-1}$ is the phonon occupation number, and $\hbar\omega_Q$ is the phonon energy. Furthermore, $|\alpha_0\rangle$ and $|\alpha_3\rangle$ are wave functions for a hole at, respectively, bound and continuum states with the corresponding energy spectra E_{α_0} and E_{α_3}. They can be determined by a Schrödinger equation regarding to the Hamiltonian H_h.

For a self-assembled GeSi QD as described in Sec. II, the finite thickness along the growth direction (taken along the z direction) is typically much narrower than the lateral extension of the electrostatic confinement along the direction per-

pendicular to the growth direction (taken along the *xy* plane). This feature has been indicated in Table I. As a result, the confining potential to a hole along the *z* direction is much stronger than that along the *xy* plane. For simplicity, in this study, we model the confinement potential along the growth direction as a narrow rectangle quantum well. Due to circular symmetry of the QD in the *xy* plane, the effective confinement has also a roughly circular symmetry in the *xy* plane.[22] This potential then can be modeled by a simple isotropic harmonic oscillator taken popularly for lateral confinement of a QD along the *xy* plane. Thus, we can use a parabolic potential for a QD in the direction perpendicular to the growth direction. Hence, the wave function and energy spectrum for a hole at a bound state in the dot can be written, respectively, as

$$|\alpha_0\rangle = |\nu\rangle = \frac{e^{im\theta}}{\sqrt{2\pi}} R_{Nm}(r)\psi_\lambda(z), \qquad (19)$$

and

$$E_{\alpha_0} = E_\nu = (2N + |m| + 1)\hbar\omega_0 + \varepsilon_\lambda. \qquad (20)$$

Here, $\mathbf{r}=(x,y)=(r,\theta)$, $\nu=(N,m,\lambda)$ refers to all quantum numbers in the dot, $m=0,\pm 1,\pm 2,\ldots$ is the angular quantum number, $N=0,1,2,\ldots$ is the radial quantum number, λ is the quantum number along the growth direction,

$$R_{mN}(r) = \frac{1}{l_0}\sqrt{\frac{2N!}{(N+|m|)!}} e^{-\rho^2/2}\rho^{|m|}L_N^{|m|}(\rho^2),$$

where $\rho=r/l_0$, $l_0=(\hbar/m^*\omega_0)^{1/2}$, and $L_N^m(x)$ is a Laguerre polynomial. The characteristic frequency of a parabolic potential in a QD can be evaluated by[20]

$$\omega_0^2 = \frac{2e^2\nu}{\pi\epsilon\epsilon_0 m^*\phi^3}, \qquad (21)$$

where ν is the filling factor of a QD which can be determined experimentally, ϕ is the diameter of a QD along the *xy* plane, and ϵ and ϵ_0 are, respectively, the material and vacuum dielectric constants. To simplify the analytical and numerical calculations, we take the usual square-well approximation to model the confining potential along the growth direction. In doing so, we have

$$\psi_\lambda(z) = (2/L)^{1/2}\sin(\lambda\pi z/L), \qquad (22)$$

and

$$\varepsilon_\lambda = \lambda^2\pi^2\varepsilon_0, \qquad (23)$$

where *L* is the height of the QD along the growth direction and $\varepsilon_0=\hbar^2/(2m^*L^2)$.

Furthermore, considering a parabolic valence-band structure in the GeSi compound, the wave function and energy spectrum for a hole in the continuum states are given, respectively, by

$$|\alpha_3\rangle = |\mathbf{K}\rangle = e^{i\mathbf{K}\cdot\mathbf{R}} \quad \text{and} \quad E_{\alpha_3} = E_\mathbf{K} = \frac{\hbar^2 K^2}{2m^*} + U_0, \quad (24)$$

where U_0 is height of the confining potential along the growth direction and $\mathbf{K}=(\mathbf{k},k_z)=(k_x,k_y,k_z)$ is the wave vector for a hole in a continuum state.

Applying the wave functions and energy spectra for a GeSi-based QD to the electronic transition rate induced by hole-phonon scattering, we have

$$W(\nu;\mathbf{K}) = \frac{2\pi}{\hbar}\sum_\mathbf{Q}\begin{bmatrix}N_Q\\N_Q+1\end{bmatrix}|V_\mathbf{Q}|^2 R_\lambda(L|k_z+q_z|)$$
$$\times S_{Nm}(l_0|\mathbf{k}+\mathbf{q}|)\delta(E_\nu - E_\mathbf{K}\pm\hbar\omega_Q) \qquad (25)$$

for transition from a bound state $|\nu\rangle$ to a continuum state $|\mathbf{K}\rangle$, and

$$W(\mathbf{K};\nu) = \frac{2\pi}{\hbar}\sum_\mathbf{Q}\begin{bmatrix}N_Q\\N_Q+1\end{bmatrix}|V_\mathbf{Q}|^2 R_\lambda(L|k_z-q_z|)S_{Nm}$$
$$\times(l_0|\mathbf{k}-\mathbf{q}|)\delta(E_\mathbf{K} - E_\nu\pm\hbar\omega_Q) \qquad (26)$$

for transition from a continuum state $|\mathbf{K}\rangle$ to a bound state $|\nu\rangle$. Here, $\mathbf{k}=(k_x,k_y)$, $\mathbf{q}=(q_x,q_y)$,

$$R_\lambda(x) = 4L(\lambda\pi)^2\frac{1-(-1)^\lambda\cos x}{[(\lambda\pi)^2 - x^2]^2},$$

and

$$S_{Nm}(y) = \frac{4\pi l_0^2 N!}{(N+|m|)!}y^{2|m|}e^{-y^2}[L_N^{|m|}(y^2)]^2.$$

C. Emission and capture rates

In a GeSi-based structure, the hole-phonon scattering is mainly achieved by interaction with acoustic-phonon modes via deformation-potential coupling.[23] In such a case, the strength of the hole-phonon coupling is

$$|V_\mathbf{Q}|^2 = (\hbar Q/2\rho)(\Xi_L^2/u_L + \Xi_T^2/u_T),$$

corresponding to the intravalley scattering,[24] where ρ is the density of the material, u_L and u_T are, respectively, the longitudinal and transverse sound velocities, and $\Xi_L=\Xi_d+\Xi_u\cos^2\theta$ and $\Xi_T=\Xi_u\cos\theta\sin\theta$, with Ξ_d and Ξ_u being, respectively, the dilatation and uniaxial deformation potentials and θ an angle to the *z* axis (i.e., $\cos\theta=q_z/Q$ and $\sin\theta=q/Q$). Here, we have included the contributions from both longitudinal and transverse acoustic-phonon couplings and $\omega_Q=u_L Q$ or $\omega_Q=u_T Q$ is the corresponding phonon frequency. In the present study, we consider a situation where the measurement is carried out at a relatively high-temperature so that $\hbar\omega_Q\ll k_B T$. For case where the transfer of holes is achieved along the growth direction with a strong confinement, the condition $|E_\mathbf{K}-E_\nu|\gg\hbar\omega_Q$ can be satisfied. Thus, using Eqs. (14) and (15), the emission and capture rates induced by hole–acoustic-phonon scattering in a QD are obtained, respectively, as

$$\lambda_E = \frac{m^* k_B T}{2\pi^4 \hbar^3 \rho Q_0} \sum_\nu \Theta(E_\nu - U_0) e^{-E_\nu/k_B T}$$

$$\times \int_0^\infty dq\, q\, S_{Nm}(l_0 q) \int_{-\infty}^\infty dq_z R_\lambda(q_z) F_-(q,q_z) \quad (27)$$

and

$$\lambda_C = \frac{m^* k_B T}{2\pi^4 \hbar^3 \rho N_3 V} \sum_\nu \Theta(E_\nu - U_0) e^{-E_\nu/k_B T}$$

$$\times \int_0^\infty dq\, q\, S_{Nm}(l_0 q) \int_{-\infty}^\infty dq_z R_\lambda(q_z) F_+(q,q_z), \quad (28)$$

where $Q_0 = 2\Sigma_\nu e^{-E_\nu/k_B T}$ is the hole number in the bound states in a dot, $N_3 = 2\Sigma_{\mathbf{K}} e^{-E_{\mathbf{K}}/k_B T}$ is the hole density in the continuum states in the system,

$$F_\pm(q,q_z) = \frac{2\pi a \Xi_u^2}{u_L^2} \left[\frac{\Xi_d^2}{\Xi_u^2} - \frac{B^* A_\pm}{128 a Q^9} + \frac{C}{96 Q^8} \right],$$

$$a = \sqrt{2m^*(E_\nu - U_0)/\hbar^2}, \quad Q = \sqrt{q^2 + q_z^2}, \quad B^* = (Q^2 - a^2)^2 B,$$

$$A_\pm = \log \frac{a^2 q_z + q_z Q^2 \pm Q(a^2 + Q^2 + 2aQ \mp 2aq_z)}{a^2 q_z + q_z Q^2 \pm Q(a^2 + Q^2 - 2aQ \pm 2aq_z)},$$

$$B = q^2(24a^2 q_z^2 - 11a^2 q^2 - 3q^2 Q^2)X^* + 8(q^6 - 3q^2 q_z^4 - 2q_z^6)\Xi^*$$
$$+ [3q^4(a^2 + q^2) + 3q^2 q_z^2(Q^2 - 8a^2) + 8q_z^4(a^2 - Q^2)], \quad (29)$$

with $X^* = (u_L/u_T)^2$, $\Xi^* = \Xi_d/\Xi_u$, and

$$C = [3q^4(-3a^4 + 6a^2 q^2 + q^4) + 6(12a^4 q^2 - 19a^2 q^4 + 15q^6)q_z^2$$
$$+ (-24a^4 - 92a^2 q^2 + 171q^4)q_z^4 + (40a^2 + 84q^2)q_z^6]X^*$$
$$+ 24[q^2 + q_z^2]^2[q^2(a^2 + q^2) + (-2a^2 + 7q^2)q_z^2 + 6q_z^4]\Xi^*$$
$$+ [9a^4 q^4 - 6a^2 q^6 + 9q^8 + (-72a^4 q^2 + 114a^2 q^4 + 18q^6)q_z^2$$
$$+ (24a^4 + 56a^2 q^2 + 81q^4)q_z^4 - 16(4a^2 - 9q^2)q_z^6 + 72q_z^8].$$

D. Further considerations

In this study, we consider the contributions to the AS from both light and heavy holes in the GeSi QDs. Due to the diffusion of Si into Ge QD during the MBE growth, the content of Ge in the GeSi dots can be estimated reasonably by popularly used methods proposed previously.[25,26] We find that for samples A, B, and C described in Sec. II, the Ge content is $x=0.75$, as shown in Table I. The value of energy band offset on the alignment of valence band along the growth direction is[25] $E_v = U_0 = 0.75x$ eV. The effective masses for heavy and light holes and the relative dielectric constant for material $Ge_x Si_{1-x}$ can be evaluated by the linearly interruption with the Ge content x through[26,27]

TABLE II. Material parameters (Ref. [27–29]).

Quantity	Symbol	Value	Unit
Longitudinal sound velocity	u_L	5247	m/s
Transverse sound velocity	u_T	3267	m/s
Dilatation deformation potential (Ge)	Ξ_d	2.0	eV
Uniaxial deformation potential (Ge)	Ξ_u	−2.16	eV
Density (Ge)	ρ	5.323	g/cm³

$$\begin{bmatrix} m_h \\ m_l \end{bmatrix} \Big/ m_0 = \begin{bmatrix} -2.8369 \\ -0.1432 \end{bmatrix} x^3 + \begin{bmatrix} 4.6844 \\ 0.3618 \end{bmatrix} x^2 + \begin{bmatrix} -2.8700 \\ -0.3669 \end{bmatrix} x$$
$$+ \begin{bmatrix} 0.8956 \\ 0.2534 \end{bmatrix},$$

and

$$\epsilon = 11.7 + 4.5x.$$

In the calculation, we take the width of the quantum well L along the growth direction to be the QD height shown in Table I and the diameter of the QD ϕ along the xy plane to be the QD diameter shown in Table I as well. The characteristic frequency ω_0 of a QD is evaluated using Eq. (26) in which the QD diameter ϕ and filling factor ν are determined experimentally (see Sec. II). The volume of a dot is also calculated using L and ϕ. Moreover, other material parameters taken in the calculations for hole-phonon scattering are listed in Table II.

IV. RESULTS AND DISCUSSIONS

In Fig. 1, we show experimental and theoretical results of the admittance spectroscopy for three QD samples with different dot sizes at a fixed ac field frequency $f = 1$ MHz. With the increasing size of the dot, the peak of the conductance shifts to higher temperature. The peak positions and half-widths for three samples A, B, and C are shown in Table I for experimental and theoretical values. As can be seen, with increasing the dot size the half-width of the conductance peak increases.

The results obtained from numerical calculations indicate that the emission rate λ_E given by Eq. (27) is about 2–3 orders of amplitude larger than the capture rate λ_C given by Eq. (28). Thus, we can take $\lambda_E \gg \lambda_C$ and use Eq. (1) to find out the emission rate experimentally. In Fig. 2, the experimental and theoretical results of the emission rate are plotted as a function of temperature for different samples A, B, and C. To determine experimentally the emission rate for a QD sample, we measure the conductance as a function of temperature for different frequencies of the ac fields. The emission rate λ_E is then the ac field frequency $\omega = 2\pi f$ at the temperature corresponding to the peak of the conductance. Theoretically, λ_E is calculated using Eq. (27). We see from

Fig. 2 that with increasing the QD size the emission rate decreases and with increasing temperature the emission rate increases rapidly.

From Eq. (27), we see that theoretically the emission rate of a GeSi QD is in a form of $\lambda_E = \beta T \Sigma_\nu \exp(-E_\nu/k_B T)$, with β being a coefficient independent on temperature. This implies that the emission rate can also be written as $\lambda_E = \beta T \exp(-E_a/k_B T)$, with E_a being the activation energy of the carriers. Thus, using the results shown in Fig. 2, the activation energy can be determined experimentally by Arrhenius plot. The Arrhenius plot is shown in Fig. 3 for three QD samples A, B, and C, where the corresponding theoretical results are also presented for comparison. We see that with increasing the QD size, the activation energy increases.

As shown in Figs. 1–3, the theoretical results for temperature dependence of the conductance and emission rate along with the Arrhenius plot for different samples are quite in line with those measured experimentally. In samples A, B, and C, the Ge content in the dot is almost the same $x \simeq 0.75$ so that the energy barrier for heavy and light holes along the growth direction U_0 is almost the same. In such a case, a larger QD height along the z direction L corresponds to the lower subband energies along the growth direction [see Eq. (28)]. It can be seen from Table I that for samples A, B, and C, the QD height along the z direction is $L = 30$, 35, and 45 Å. Because the AS measured here is induced by electronic transition along the growth direction, the lower hole subband energies imply that the holes in the bound states in a dot need more energy to overcome the energy barrier U_0 to be emitted into the continuum states. Together with the fact that the lower energy subbands are more possibly occupied by holes, with increasing size of the dots the peak of the conductance shifts to the high-temperature regime, the emission rate decreases and the activation energy increases. In GeSi-based QD systems, the electron–acoustic-phonon scattering via deformation potential coupling is the principal channel for electronic transition between the bound states in the dot and the continuum states in the systems. Under the action of an ac field, holes in the QD can gain the energy from this driving field and loss the energy via hole-phonon scattering and via electronic transition from lower-energy bound states to the higher-energy continuum states. Because phonon occupation number increases with temperature, the strength of hole-phonon scattering increases with T and, consequently, the emission rate increases rapidly with increasing temperature.

The obtained experimental and theoretical results indicate that the emission rate in GeSi-based QD systems is about 1–2 order of amplitude smaller than that in GeSi-based quantum wells.[12] In a GeSi QD, the confinement of hole motion in all spacial directions implies that the momentum conser-

vation law does not hold anymore during a scattering event. Thus, the hole-phonon scattering can only occur among the quantized energy levels so that the effective hole-phonon scattering can be reduced in a QD. This is the main physics reason behind a lower emission rate observed in a QD than in a quantum well. Furthermore, the theoretical and experimental results suggest that in a GeSi QD, the emission rate is in a form $\lambda_E = \beta T \exp(-E_a/k_B T)$, in contrast to $\lambda_E = \beta T^{1/2} \exp(-E_a/k_B T)$ for a GeSi quantum well.[12]

It should be noted that in this study, we take a single QD for theoretical modeling. In contrast, the samples used in the measurements are multidots with different areal densities (see Table I), although the nonuniformity of the QD size is less than 10% in each sample. We believe this is the main reason why the results obtained theoretically do not agree fully quantitatively with those measured experimentally. Nevertheless, our theoretical model can reproduce rightly those observed experimentally with a reasonably good agreement.

V. SUMMARY

In this study, we have examined experimentally the effect of the size of self-assembled GeSi QDs on features of admittance spectroscopy measured along the growth direction. We have found that with increasing the QD size, the peak of the conductance shifts to higher temperature, the emission rate decreases, and the activation energy increases. In conjunction with these experiments and experimental findings, we have developed a simple and systematic theoretical approach to calculate the admittance spectroscopy in GeSi-based QD systems and obtained the corresponding analytical and numerical results. Using this model calculation, we can obtain the conductance and emission rate of carriers in a QD due to the presence of the applied ac field and electronic scattering mechanisms. The proposed theoretical modeling is based on the known sample and material parameters. Thus, the obtained theoretical results are in line with those measured experimentally. We have applied the theoretical analysis to understand the experimental findings. We hope this combined experimental and theoretical study can lead to an in-depth understanding of electronic properties of GeSi-based quantum dot systems.

*wen105@rsphysse.anu.edu.au

†fanglu@fudan.edu.cn

[1] See, e.g., T. J. Thornton, Rep. Prog. Phys. **58**, 311 (1995).

[2] See, e.g., D. Loss and D. P. DiVincenzo, Phys. Rev. A **57**, 120 (1998).

[3] See, e.g., S. N. Molotkov and S. S. Nazin, JETP Lett. **63**, 687 (1996).

[4] See, e.g., H. Saito, K. Nishi, I. Ogura, S. Sugou, and Y. Sugomito,

Appl. Phys. Lett. **69**, 3140 (1996).

[5] See, e.g., D. Bimberg, M. Grundmann, and N. N. Ledentsov, *Quantum Dot Heterostructures* (Wiley, Chichester, 1998).

[6] P. N. Brunkov, A. Patané, A. Levin, L. Eaves, P. C. Main, Y. G. Musikhin, B. V. Volovik, A. E. Zhukov, V. M. Ustinov, and S. G. Konnikov, Phys. Rev. B **65**, 085326 (2002).

[7] W.-H. Chang, W. Y. Chen, T. M. Hsu, N. T. Yeh, and J. I. Chyi, Phys. Rev. B **66**, 195337 (2002).

[8] J. F. Chen, R. S. Hsiao, C. K. Wang, J. S. Wang, and J. Y. Chi, J. Appl. Phys. **98**, 013716 (2005).

[9] Fengying Yuan, Zuimin Jiang, and Fang Lu, Appl. Phys. Lett. **89**, 072112 (2006).

[10] A. I. Yakimov, A. V. Dvurechenskii, A. I. Nikiforov, A. A. Bloshkin, A. V. Nenashev, and V. A. Volodin, Phys. Rev. B **73**, 115333 (2006).

[11] F. Lu, D. Gong, J. Wang, Q. Wang, H. Sun, and X. Wang, Phys. Rev. B **53**, 4623 (1996).

[12] X. Li, W. Xu, F. Y. Yuan, and F. Lu, Phys. Rev. B **73**, 125341 (2006).

[13] A. Ishizaka and Y. Shiraki, J. Electrochem. Soc. **133**, 666 (1986).

[14] Jeff Drucker, IEEE J. Quantum Electron. **38**, 975 (2002).

[15] A. V. Dvurechenskii, J. V. Smagina, R. Groetzschel, V. A. Zinovyev, V. A. Armbrister, P. L. Novikov, S. A. Teys, and A. K. Gutakovskii, Surf. Coat. Technol. **196**, 25 (2005).

[16] J. Drucker, IEEE J. Quantum Electron. **38**, 975 (2002).

[17] F. Cerdeira, A. Pinczuk, J. C. Bean, and B. A. Wilson, Appl. Phys. Lett. **45**, 1138 (1984).

[18] V. I. Mashanov, H.-H. Cheng, C.-H. Chia, and Y.-H. Chang, Physica E (Amsterdam) **28**, 531 (2005).

[19] QiJia Cai, Hao Zhou, and Fang Lu, Appl. Surf. Sci. **253**, 4792 (2006).

[20] M. Koskinen, M. Manninen, and S. M. Reimann, Phys. Rev. Lett. **79**, 1389 (1997).

[21] W. Xu, Phys. Rev. B **57**, 12939 (1998); W. Xu, F. M. Peeters, and J. T. Devreese, *ibid.* **46**, 7571 (1992).

[22] S. M. Reimann and M. Manninen, Rev. Mod. Phys. **74**, 1283 (2002).

[23] H. Mizuno, K. Taniguchi, and C. Hamaguchi, Phys. Rev. B **48**, 1512 (1993).

[24] C. Jacoboni and L. Reggiani, Rev. Mod. Phys. **55**, 645 (1983).

[25] R. Magalhães-Paniago, G. Medeiros-Ribeiro, A. Malachias, S. Kycia, T. I. Kamins, and R. S. Williams, Phys. Rev. B **66**, 245312 (2002).

[26] Karl Brunner, Rep. Prog. Phys. **65**, 27 (2002).

[27] Lianfeng Yang, J. R. Watling, R. C. W. Wilkins, M. Boric, J. R. Barker, A. Asenov, and S. Roy, Semicond. Sci. Technol. **19**, 1174 (2004).

[28] M. V. Fischettia and S. E. Laux, J. Appl. Phys. **80**, 2234 (1996).

[29] F. Schaffler, in *Properties of Advanced Semiconductor Materials: GaN, AlN, InN, BN, SiC, SiGe*, edited by M. E. Levinshtein, S. L. Rumyantsev, and M. S. Shur (Wiley, New York, 2001), pp. 149–188.